Data Supplement for Krivinko et al., Synaptic Proteome Compensation and Resilience to Psychosis in Alzheimer's Disease. Am J Psychiatry (doi: 10.1176/appi.ajp.2018.17080858)

Appendices

Appendix 1. Subjects

We studied a total of 140 AD subjects (Table 1 in the main text) through the brain bank of the Alzheimer Disease Research Center (ADRC) at the University of Pittsburgh, using protocols approved by the University of Pittsburgh Institutional Review Board and Committee for Oversight of Research and Clinical Training Involving Decedents. All cases coming to autopsy between 1993 and 2014 with a primary neuropathologic diagnosis of Alzheimer's disease and a Braak stage between 3-5 were included in the study. End-stage cases, as defined by a Braak stage of 6, were excluded. Subjects underwent comprehensive evaluations by experienced clinicians in the ADRC, including neurologic, neuropsychological, and psychiatric assessments as previously described (1–3). Using this information, information obtained from clinical records, and structured interviews with surviving relatives, an independent committee of experienced clinicians made consensus DSM-IV diagnoses for each subject. Psychosis was defined as the presence of delusions or hallucinations at any visit. Subjects with a preexisting psychotic disorder (e.g. schizophrenia) were excluded from the study.

Normal control subject brain specimens were obtained through the ADRC as described above and additionally through the Allegheny County Medical Examiner's Office. For the latter, consent was obtained from the subjects' next-of-kin. The protocol used to obtain consent was approved by the University of Pittsburgh Institutional Review Board and Committee for Oversight of Research Involving the Dead. An independent committee of experienced clinicians made consensus DSM-IV diagnoses for each subject, using information obtained from clinical records and structured interviews with surviving relatives. Samples from subjects without any DSM-IV diagnosis (i.e. including no diagnosis of a cognitive disorder) were used in this study.

Appendix 2. Human sample collection and neuropathologic assessment

For ADRC subjects, postmortem interval (PMI) was recorded at the time of brain removal. At autopsy, the brain was removed intact, examined grossly, and divided in the midsagittal plane. Gray matter samples from the right superior frontal gyrus of the DLPFC were dissected and frozen at −80 °C. The left hemibrain was immersion fixed in 10% buffered formalin for at least one week, sectioned into 1.0 cm coronal slabs, and sampled according to Consortium to Establish a Registry for Alzheimer's Disease (CERAD) protocol for neuropathological diagnosis of AD (4) or, since 2012, following National Institute of Aging – Alzheimer's Association (NIA-AA) guidelines (5). AD pathology was evaluated using the modified Bielschowsky silver stain (6) and immunohistochemical staining for tau and amyloid β. Neuritic plaque density was assessed according to CERAD criteria (4); distribution of tau pathology was classified according to Braak stages (7). Lewy body pathology was assessed by alpha-synuclein immunohistochemistry, and positive cases were classified into amygdala-predominant, limbic/neocortical-predominant, or other categories (Table S1), a modified scheme based on consensus criteria (5, 8). Immunohistochemical staining for phospho-TDP-43 was performed on sections of amygdala, hippocampus, mesial temporal cortex and middle frontal gyrus as previously described (9). Sections were evaluated for the absence or presence of TDP-43 positive neuronal cytoplasmic inclusions, neuronal intranuclear inclusions and dystrophic neurites. Based on the distribution of

TDP-43 pathology, positive cases were classified into amygdala-predominant, mesial temporal, neocortical, or in cases when amygdala sections were not available but all other sections were TDP-43 negative, indeterminate categories (Table S1).

TABLE S1. Univariate analyses of Lewy body and TDP-43 pathology from AD subjects with and without psychosis whose tissue was utilized for quantitative immunohistochemistry

Variable	AD-P (n=59)	AD+P (n = 81)	p value
Lewy body pathology:			0.36
negative	33 (56%)	34 (42%)	
amygdala	7 (12%)	10 (12%)	
limbic/neocortical	18 (31%)	33 (41%)	
other	1 (2%)*	4 (5%)**	
TDP-43 pathology:			0.19
negative	30 (51%)	27 (33%)	
amygdala	7 (12%)	16 (20%)	
mesial temporal	14 (24%)	22 (27%)	
neocortical	4 (7%)	12 (15%)	
indeterminate/missing	4 (7%)	4 (5%)	

Results are reported as “n (% of group total).”
*1 subject with incomplete tissue sectioning
**pathology present only in brainstem (1) or olfactory (1) areas. 2 subjects with incomplete tissue sectioning.

Assessment of vascular pathology included atherosclerosis of the circle of Willis, arteriolosclerosis in frontal white matter and cerebral amyloid angiopathy in DLPFC. Each was rated as none (0), mild (1), moderate (2) or severe (3), and a sum score was generated by adding the three individual scores. Microvascular lesions (MVL) were defined as remote microinfarcts/microhemorrhages not seen on gross examination and less than 1.0 cm in size. MVLs were enumerated in standardized sections (5) of middle frontal gyrus (DLPFC), superior and middle temporal gyrus, inferior parietal lobule, occipital cortex (BA 17/18), basal ganglia at level of anterior commissure, and thalamus at the level of the subthalamic nucleus to create MVL counts.

Neuropathologic diagnoses of Alzheimer disease were made according to CERAD criteria (4), although all AD subjects also met NIA-Reagan criteria (10) for intermediate to high probability that their dementia was due to AD lesions.

For normal control subjects, samples from the frontal pole, hippocampus, entorhinal cortex, and cerebellum were collected at time of autopsy and an experienced neuropathologist reviewed sections stained using hematoxylin and eosin, Bielschowsky silver stain, and amyloid β immunohistochemistry to confirm that there was no evidence of neurodegenerative disease. The right hemisphere was blocked coronally at 1-2 cm intervals and the resultant slabs snap frozen in 2-methyl butane on dry ice, and stored at -80 °C. Tissue slabs containing the DLPFC were identified. From these slabs, DLPFC was removed as single blocks. Gray matter was collected by cutting 40 μM sections and frozen at −80 °C.

Appendix 3. Quantitative Immunohistochemistry

Serial 5 μm thick formalin-fixed, paraffin-embedded tissue sections were immunostained on an automated stainer (Discovery Ultra, Ventana, Tucson, AZ) using the following primary antibodies: PHF-1 (1:1000, kindly provided by Peter Davies), oligomeric tau T22 (1:500, EMD Millipore, Billerica, MA), beta-amyloid NAB228 (1:4000 (Cell Signaling Technology, Danvers, MA), after 40 min pretreatment with 90% formic acid), and microglial markers Iba1 (1:500, Wako, Richmond, VA) and HLA-DR (1:100, Dako, Agilent Technologies, Santa Clara, CA). Except for beta-amyloid, slides for all other stains were pretreated with Discovery CC1 solution, a Tris based buffer with a slightly basic pH (Ventana Medical Systems, Tucson, AZ). All slides were developed using a multimeric HRP/DAB detection system (Ventana Medical Systems, Tucson, AZ). No counterstaining was performed to ease signal quantification. For double fluorescent immunohistochemistry of PHF-1 (1:500) and T22 (1:1000) (Figure S1), T22 staining was followed by tyramine signal amplification (Perkin Elmer, Waltham, MA).

FIGURE S1. Representative images of DLPFC sections double-labeled for PHF-1 and oligomeric (T22) tau

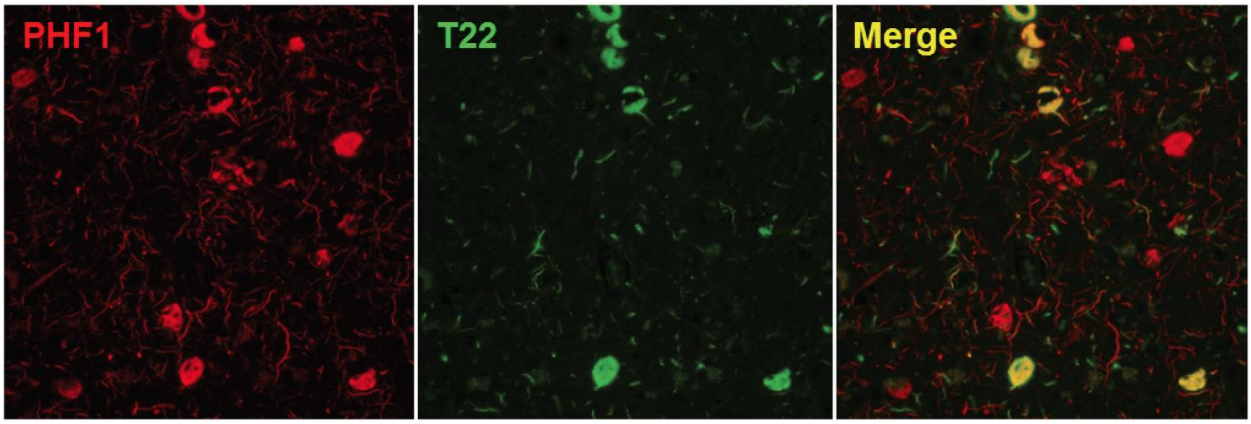

Dual immunohistochemical labeling of PHF-1 (red, left panel) and oligomeric (green, middle panel) tau reveals a tau population which is highly correlated, but not redundant (yellow, right panel).

Appendix 4. Microscopy

Whole slide digital images of the immunostained sections were created using a Mirax MIDI slide scanner (Zeiss, Jena, Germany) at 40x resolution (0.116 micron/pixel). Digital image analysis was performed using NearCyte software (Andrew Lesniak, University of Pittsburgh). For each section, 4 rectangular regions of interest (ROI) of 4mm^2 were created. These ROIs were defined to span the entire cortical thickness and were preferentially placed midway along the gyral axis to avoid tangentially cut cortical regions (Figure S2). Minor manual adjustments were made to adapt to curvatures and irregularities in the cortical ribbon. Once placed for the first analyzed stain (PHF-1), the same ROIs were re-used for all subsequent stains. If tissue folds or other artifacts prevented placement in the same location, the ROI was moved to an acceptable site as close as possible to the original location. For quantitative image analysis, thresholds for signal positivity were optimized manually for each stain and then maintained constant throughout the analysis of all slides (Figure 1 in the main text). Signals from all four ROIs were integrated into two outcome variables: area ratio (= positive area/entire field area) and mean signal intensity. For HLA-DR and Iba1 stains, an additional variable, the HLA-DR/Iba1 ratio was derived to normalize microglial activation (HLA-DR) to microglial density (Iba1). All analyses were done blinded to psychosis status.

FIGURE S2. Tissue sampling approach for quantitative immunohistochemistry

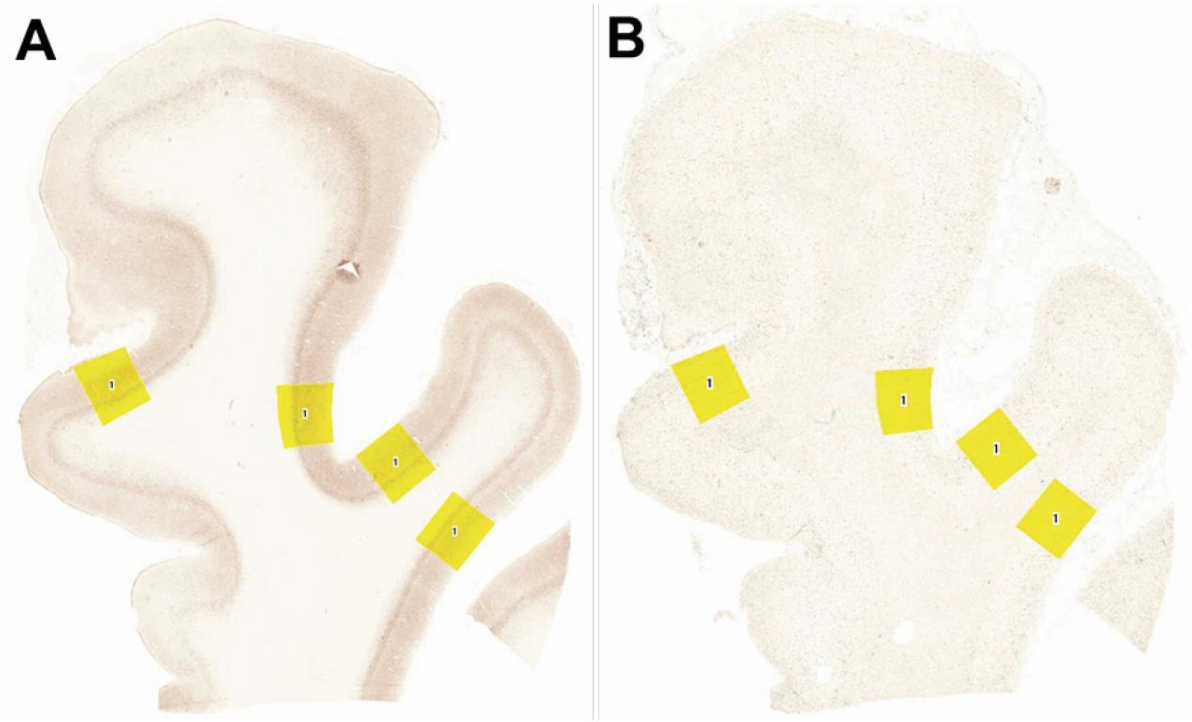

Representative whole slide images demonstrating the selection of four cortical regions of interest (ROI), each measuring 4 mm^2 and spanning the entire cortical thickness. ROIs were preferentially placed midway along the gyrus, and tangentially cut cortical regions were avoided. ROIs were first defined for PHF-1 stained slides (A) and then re-used for all other stains done on adjacent tissue sections (e.g. Iba1) (B).

Appendix 5. Animals

APPswe/PSEN1dE9 mice with transgenes encoding mutant presenilin and amyloid precursor protein (B6.Cg-Tg(APPswe,PSEN1dE9)85Dbo/Mmjax) were developed by Dr. David Borchelt, McKnight Brain Institute, University of Florida (11, 12). The APPswe transgene contains cDNA for a chimeric APP whose sequence encoding the Aβ domain has been replaced with the human sequence encoding Swedish mutations K595N/M596L. The PSEN1dE9 transgene contains cDNA for human PSEN1 containing a deletion of exon 9, the deltaE9 mutation. Both transgenes are inserted at a single locus between Arpp21 and Pdcd6ip on chromosome 9 and controlled by mouse prion promoter. Each breeding pair consisted of 1 APPswe/PSEN1dE9 male and 1 wildtype female littermate, both of which were ordered from Mutant Mouse Regional Resource Center - University of Missouri (Stock #034832-JAX), and obtained from The Jackson Laboratories (JAX, Bar Harbor, ME) with mice cogenic on a C57Bl/6J background (N17). To maintain this line, female mice, either littermates of APPswe/PSEN1dE9 males or obtained from JAX, were bred with APPswe/PSEN1dE9 males.

Mice heterozygous for deletion of the *Kalrn* gene were developed at Northwestern University by Dr. Peter Penzes and were generated from embryonic stem cells by inGenious Targeting Laboratory (Ronkonkoma, NY) (13), in which exons 27-28 and the intervening intron were

replaced with a neo cassette under an independent PGK promoter. Mice containing this deletion on a C57Bl/6NCR background were shipped to JAX, where they were re-derived on a C57Bl/6NJ background, before being shipped to University of Pittsburgh. A line of *Kalrn* underexpressors was then maintained at University of Pittsburgh by breeding males heterozygous for *Kalrn* deletion to wildtype C57Bl/6J females from JAX.

APPswe/PSEN1dE9 males were then mated to *Kalrn*+/- females at University of Pittsburgh to obtain four genotypes as previously described (14): APPswe/PSEN1dE9/*Kalrn*+/+ (APP/PS1/KALRN(+/+)), APPswe/PSEN1dE9/*Kalrn*+/- (APP/PS1/KALRN(+/-)), *Kalrn*+/+ (WT), and *Kalrn*+/-. At postnatal day 14 (P14), male pups produced from the *Kalrn*+/-, APP/PS1/KALRN(+/+) cross were numbered with ear tags and genotyped from tail snips. Mice were then weaned into cages with 2-4 mice per cage at P21-23.

At 5-6 months of age, mice were weighed and deeply anesthetized with a 150 mg/kg intraperitoneal injection of pentobarbital. Mice were then perfused with 10 mL ice-cold normal saline transcardially before rapid decapitation and brain extraction. The right cerebral cortex was separated from surrounding brain tissue by gross dissection and immediately frozen on dry ice.

Appendix 6. Animal tissue preparation for LC-MS/MS

Samples were then homogenized with a Teflon pestle in 1 mL of a solution containing 0.32 M sucrose, 1 mM $MgCl_2$, 0.1 mM $CaCl_2$, and 5 mM NaF with protease and phosphate inhibitors. 40 µL of this homogenate was put aside in 2% SDS, bath sonicated, clarified by centrifugation, and used for LC-MS/MS to assay synaptic protein levels in whole-cell homogenates. The remaining homogenate was clarified by centrifugation at 800g for 10 minutes, the supernatant was obtained, and the solution was adjusted to a final volume/sucrose concentration of 2 mL and 1.25 M. The tissue solution was pipetted onto a 5 ml layer of 1.5 M sucrose and separated by ultracentrifugation at 100,000g for 3 hours. The synaptosome fraction was retrieved from the interface between the 1.25 M and 1.5 M sucrose layers, diluted 1:10 with 0.05 mM $CaCl_2$ with protease and phosphatase inhibitors, and centrifuged at 60,000g for 20 min. The synaptosome pellet was then dissolved in resuspension buffer with 20 mM Tris-HCl (pH 8), and 1% triton (along with protease and phosphatase inhibitors), and agitated on a rocker at 4 °C for 90 minutes. Samples were then separated by ultracentrifugation for 30 minutes at 113,000g. The presynaptic fraction was saved and the pellet containing the postsynaptic density enrichment was resuspended in 10 mM Tris-HCl (pH 7.4) with 2% SDS. Protein concentration was assayed with a Micro BCA Protein Assay Kit (Thermo Fisher Scientific). Samples were then analyzed by LC-MS/MS as described above.

Appendix 7. Statistical Analysis of mouse protein data.

To compare APP/PS1/KALRN(+/-) and APP/PS1/KALRN(+/+) mice within homogenate and PSD fractions, protein ratios were calculated either between APP/PS1/KALRN(+/-) and APP/PS1/KALRN(+/+) mice, or relative to WT mice. One-sample t-tests (of log2 ratios) were conducted to detect shifts in the distributions of synaptic protein levels. Finally, a two-way ANOVA was performed on the relative-to-WT protein ratios (with genotype, compartment, and genotype-by-compartment interactions) to evaluate these effects on synaptic protein levels.

Additional Supplementary Tables

Tables S3 and S5 are below. Tables S2, S4, S6, and S7 are in supplementary Excel files.

TABLE S3. Gene ontology terms for the top 20 proteins with the greatest increase in fold change in AD-P vs control subjects

Term	Genes	p value
GO:0016020~membrane	NCAM1, EEF1A1, HSPA2, NCDN, PPIA, FLOT2, FLOT1, SEC22B, VAMP2, STX1B, GAPDH	7.72E-06
GO:0005829~cytosol	EEF1A1, HSPA2, NCDN, PPIA, VAMP2, STX1B, GAPDH, PRDX1, CALB2, ADD2	1.60E-03
GO:0031410~cytoplasmic vesicle	FLOT2, FLOT1, VAMP2, ADD2	2.16E-03
GO:0005913~cell-cell adherens junction	FLOT2, FLOT1, PRDX1, SEPT9	3.42E-03
GO:0005634~nucleus	EEF1A1, HSPA2, NCDN, PPIA, STX1B, GAPDH, PRDX1, CALB2	1.48E-02
GO:0031982~vesicle	FLOT2, VAMP2, GAPDH	1.52E-02
GO:0031201~SNARE complex	SEC22B, VAMP2, STX1B	2.10E-02
GO:0005737~cytoplasm	NCAM1, EEF1A1, GLUD1, STX1B, GAPDH, PRDX1, CALB2, SEPT9	2.34E-02
GO:0030864~cortical actin cytoskeleton	EEF1A1, FLOT2, FLOT1	2.92E-02
GO:0048471~perinuclear region of cytoplasm	FLOT2, VAMP2, GAPDH, SEPT9	3.59E-02
GO:0005886~plasma membrane	NCAM1, NCAM2, FLOT2, FLOT1, GRIN2A, VAMP2, STX1B, GAPDH, ADD2	3.71E-02
GO:0005815~microtubule organizing center	FLOT1, STX1B	4.02E-02
GO:0042470~melanosome	FLOT1, SEC22B, PRDX1	4.61E-02

Pathway analysis used the Database for Annotation, Visualization and Integrated Discovery (DAVID) Functional Annotation Tool (15, 16) and searched for gene ontology term enrichment. Proteins were tested for enrichment relative to the 190 proteins assayed in homogenate, rather than against the entire genome, to increase stringency.

TABLE S5. Gene ontology terms for the top 20 non-PSD-enriched proteins with elevated levels in cortical homogenates from resilient APP/PS1/KALRN(+/-) mice

Term	Genes	p value
GO:0016023~cytoplasmic membrane-bounded vesicle	*AP2B1, AP2A2, HSP90AA1, DMXL2, ATP1A1, HSPA5, SV2A, CLTC*	5.53×10^{-6}
GO:0031988~membrane-bounded vesicle	*AP2B1, AP2A2, HSP90AA1, DMXL2, ATP1A1, HSPA5, SV2A, CLTC*	6.84×10^{-6}
GO:0031410~cytoplasmic vesicle	*AP2B1, AP2A2, HSP90AA1, DMXL2, ATP1A1, HSPA5, SV2A, CLTC*	1.53×10^{-5}
GO:0031982~vesicle	*AP2B1, AP2A2, HSP90AA1, DMXL2, ATP1A1, HSPA5, SV2A, CLTC*	2.02×10^{-5}
GO:0048770~pigment granule	*HSP90AA1, ATP1A1, HSPA5, CLTC*	2.47×10^{-4}
GO:0042470~melanosome	*HSP90AA1, ATP1A1, HSPA5, CLTC*	2.47×10^{-4}
GO:0030136~clathrin-coated vesicle	*AP2A2, DMXL2, SV2A, CLTC*	7.84×10^{-4}
GO:0030659~cytoplasmic vesicle membrane	*AP2B1, AP2A2, SV2A, CLTC*	9.11×10^{-4}
GO:0012506~vesicle membrane	*AP2B1, AP2A2, SV2A, CLTC*	1.16×10^{-3}
GO:0030135~coated vesicle	*AP2A2, DMXL2, SV2A, CLTC*	1.34×10^{-3}
GO:0044433~cytoplasmic vesicle part	*AP2B1, AP2A2, SV2A, CLTC*	2.14×10^{-3}
GO:0030665~clathrin coated vesicle membrane	*AP2A2, SV2A, CLTC*	2.47×10^{-3}
GO:0012505~endomembrane system	*AP2B1, AP2A2, ATP2A2, HSPA5, SV2A, CLTC*	3.71×10^{-3}
GO:0030662~coated vesicle membrane	*AP2A2, SV2A, CLTC*	4.64×10^{-3}

Pathway analysis used the Database for Annotation, Visualization and Integrated Discovery (DAVID) Functional Annotation Tool (15, 16) and searched for gene ontology term enrichment. The 20 proteins with the most altered levels in APP/PS1/KALRN(+/-) compared to APP/PS1/KALRN(+/+) were tested for enrichment relative to the 174 proteins assayed in homogenate, rather than against the entire genome, to increase stringency. Proteins defined as “PSD-enriched” were excluded for the analysis. Terms reported were contained within the annotation cluster with the greatest enrichment score.

References

1. Sweet RA, Hamilton RL, Lopez OL, Klunk WE, Wisniewski SR, Kaufer DI, et al. Psychotic symptoms in Alzheimer's disease are not associated with more severe neuropathologic features. Int Psychogeriatr. 2000;12(4):547-58.
2. Lopez OL, Becker JT, Chang YF, Sweet RA, Aizenstein H, Snitz B, et al. The long-term effects of conventional and atypical antipsychotics in patients with probable Alzheimer's disease. Am J Psychiatry. 2013;170(9):1051-8.
3. Murray PS, Kirkwood CM, Gray MC, Ikonomovic MD, Paljug WR, Abrahamson EE, et al. beta-Amyloid 42/40 ratio and kalirin expression in Alzheimer disease with psychosis. Neurobiol Aging. 2012;33(12):2807-16.
4. Mirra SS, Heyman A, McKeel D, Sumi SM, Crain BJ, Brownlee LM, et al. The Consortium to Establish a Registry for Alzheimer's Disease (CERAD). Part II. Standardization of the neuropathologic assessment of Alzheimer's disease. Neurology. 1991;41(4):479-86.
5. Montine TJ, Phelps CH, Beach TG, Bigio EH, Cairns NJ, Dickson DW, et al. National Institute on Aging-Alzheimer's Association guidelines for the neuropathologic assessment of Alzheimer's disease: a practical approach. Acta Neuropathol. 2012;123(1):1-11.
6. Yamamoto T, Hirano A. A comparative study of modified Bielschowsky, Bodian and thioflavin S stains on Alzheimer's neurofibrillary tangles. Neuropathol Appl Neurobiol. 1986;12(1):3-9.
7. Braak H, Alafuzoff I, Arzberger T, Kretzschmar H, Del Tredici K. Staging of Alzheimer disease-associated neurofibrillary pathology using paraffin sections and immunocytochemistry. Acta Neuropathol. 2006;112(4):389-404.
8. McKeith IG, Dickson DW, Lowe J, Emre M, O'Brien JT, Feldman H, et al. Diagnosis and management of dementia with Lewy bodies: third report of the DLB Consortium. Neurology. 2005;65(12):1863-72.
9. Vatsavayi AV, Kofler J, Demichele-Sweet MA, Murray PS, Lopez OL, Sweet RA. TAR DNA-binding protein 43 pathology in Alzheimer's disease with psychosis. Int Psychogeriatr. 2014;26(6):987-94.
10. Hyman BT, Trojanowski JQ. Consensus recommendations for the postmortem diagnosis of Alzheimer disease from the National Institute on Aging and the Reagan Institute Working Group on diagnostic criteria for the neuropathological assessment of Alzheimer disease. J Neuropathol Exp Neurol. 1997;56(10):1095-7.
11. Borchelt DR, Ratovitski T, van Lare J, Lee MK, Gonzales V, Jenkins NA, et al. Accelerated amyloid deposition in the brains of transgenic mice coexpressing mutant presenilin 1 and amyloid precursor proteins. Neuron. 1997;19(4):939-45.
12. Jankowsky JL, Slunt HH, Ratovitski T, Jenkins NA, Copeland NG, Borchelt DR. Co-expression of multiple transgenes in mouse CNS: a comparison of strategies. Biomol Eng. 2001;17(6):157-65.
13. Cahill ME, Xie Z, Day M, Photowala H, Barbolina MV, Miller CA, et al. Kalirin regulates cortical spine morphogenesis and disease-related behavioral phenotypes. Proc Natl Acad Sci U S A. 2009;106(31):13058-63.
14. Krivinko JM, Erickson SL, Abrahamson EE, Wills ZP, Ikonomovic MD, Penzes P, et al. Kalirin reduction rescues psychosis-associated behavioral deficits in APPswe/PSEN1dE9 transgenic mice. Neurobiol Aging. 2017;54:59-70.
15. Huang da W, Sherman BT, Lempicki RA. Bioinformatics enrichment tools: paths toward the comprehensive functional analysis of large gene lists. Nucleic Acids Res. 2009;37(1):1-13.
16. Huang da W, Sherman BT, Lempicki RA. Systematic and integrative analysis of large gene lists using DAVID bioinformatics resources. Nat Protoc. 2009;4(1):44-57.